Technical Paper

Journal of the Society of Naval Architects of Korea
Vol. 27, No. 3, September 1990
大 韓 造 船 學 會 誌
第27卷 第3號 1990年 9月

Evaluation of Impact Loads Associated with Flare Slamming

by

Armin W. Troesch* and Chang-Gu Kang**

플레어 슬래밍에 관련된 충격하중의 계산

Armin W. Troesch*, 강 창 구**

Abstract

The hydrodynamic aspects of bow flare impact are discussed and the assumptions implicit in typical flare impact calculations are examined. Calculations based upon a pressure release free surface boundary condition are presented. While this simplified boundary condition eliminates the possibility of important factors such as splash-up and above-surface wetting, it has the significant advsntage of being computationally simple. Both three-dimensional and two-dimensional results are compared with experiments. Errors resulting from the approximate free surface condition are examined. Also included in the two-dimensional and three-dimensional analysis are longitudinal distributions of the vertical bending moment and vertical shear force.

요 약

본 논문에서는 유체동력학적면에서 선수 플레어 충격에 대하여 고찰하고, 특히 전형적인 플레어 충격하중 계산에서 사용된 가정에 대하여 검토한다.

압력이 작용하지 않는 자유표면 경계조건에 의한 계산결과들이 제시된다. 이 단순화된 경계조건을 사용하면 물이 제트처럼 올라오는 현상이나 평균자유표면 위의 젖은 부분과 같은 중요한 인자를 무시하게 되지만, 계산할 때는 아주 단순하다는 장점을 갖는다. 3차원 계산결과와 2차원 계산 결과를 실험과 비교하였으며, 근사 자유 표면 조건으로부터 발생하는 오차를 검토 하였다. 또, 2차원 및 3차원 해석에서 연직 굽힘 모멘트와 연직 전단력도 포함되었다.

1. Introduction

The structural response of a ship in a severe seaway has been the subject of many studies over the years. When the relative motion between the ship and water surface exceed some threshold level, large impact forces will occur. Recent reports from the 8th and 9th International Ship Structures Congress (ISSC[27] and ISSC[28]) describe many of the state-of-the-art methods used in the prediction and analysis of ship impact. These reports conclude that

Manuscript received: June 4, 1990, revised manuscript received: August 2, 1990
* The University of Michigan, Dept. of Naval Architecture & Marine Engineering
** Member, Korea Research Institute of Ships and Ocean Engineering

there are still many unanswered questions involving the calculation of impact and slamming loads. In particular, issues relating to the scale effects of model tests, discrepancies between the classic drop tests and standard seakeeping experiments, and the effects of implicit assumptions in theoretical/empirical calculations go unresolved. In order to completely describe the impact force and the resulting structural response, various components, such as entrapped air, hydroelastic interaction, and nonlinear free surface mechanics, must be correctly taken into account.

Due to the complexity of the problem and due to a real need for engineering answers, the "science" of hydrodynamic impact includes a considerable amount of empiricism. For example, a large effort has been made in predicting the maximum impact pressures due to bottom slamming. Typically the expressions for the pressures are functions of hull entrance angles, relative velocities between hull and water surfaces, and empirical correction factors based upon drop test measurements. This approach has had some measure of success when compared with model seakeeping experiments and full scale data (Ochi and Motter [17] and [18]). Researchers, however, have also integrated these pressures to find the structural shear and bending moments due to impact. Example of this are Ochi and Motter[18] or Belik, et al.[6]. The integration of the empirically determined pressure implies additional assumptions about the pressure's spatial and temporal distributions. These assumptions are often not clearly stated or understood and it is not obvious that the correction factors for the peak pressures can be adjusted to correctly include all the effects that contribute to the integrated impact loads.

A special, yet important part of ship impact is the loading imposed upon the ship's structure due to above-mean-waterline shape. In numerous instances, damage has been noted in the bow and forebody regions of ships with large flare angles. The flare impact problem includes many of the same mechanisms that are found in the bottom impact problem. Both may be influenced by entrapped air, hydroelastic interaction, and nonlinear free surface mechanics. The hydrodynamic force due to initial impact, such as that found in bottom slamming, has been studied extensively. Using perturbation techniques, researchers from Wagner[24] to Armand and Cointe[2] have shown reasonable agreement for initial impact forces acting on two-dimensional cylinders. However, the extension of these zero or near zero draft theories to deep-draft flare impact may not be possible.

The purpose of this paper is to investigate the hydrodynamics of three-dimensional flare impact. Simplifying assumptions will be noted and their effects will be discussed. Comparisions between three-dimensional and two-dimensional potential flow calculations will be made. The two-dimensional analysis is based upon the standard strip theory assumptions commonly found in impact predictions. The theoretical results include the total impact force, vertical shear, and vertical bending moment for two bodies. Comparisons will be made between the calculated and experimentally measured impact forces.

2. Problem Definition

The impact pressures and loads are assumed so be due to a rigid body entering otherwise calm water. The flow will be assumed to be potential. Viscosity, surface tension, air entrapment, compressibility of air or water, and hydroelastic interaction will be ignored.

Viscosity is generally thought not to be important in vertical impact. Much of the force comes from the inertial effect of the water when the body accelerates the fluid out of the way. This, however, may not be true when horizontal impact is a factor. See Troesch and Kang[21] Figure 18, where the experimentally-measured horizontal impact component for a dropped body with forward speed rises at a significantly higher rate than the theoretical prediction. The difference of the free surface elevations at the fore and after bodies is one of the important factor for the horizontal impact.

Surface tension will certainly have an effect on the behavior of the water as it forms a spray sheet or droplets, and any analytical model that includes

splash-up should examine its effects (Lin[14]). Vessel visibility is an example of when spray or the jet-like behavior of water due to impact may be important. The impact load, though, is due to pressures acting on the actual boundary and spray sheets do not significantly contribute to these forces.

Air entrapment is a significant factor when flat or nearly flat bodies strike the water surface. Chuang and Milne[10] have demonstrated through experiments that the air trapped during drop tests provided a cushioning effect which typically reduced the maximum impact pressure. However, this phenomenon was most prevalent during experiments involving two-dimensional, flat bottom models or two-dimensional wedges with a deadrise of 1 degree or less. For wedges with deadrise of 3 degrees or more, or for three-dimensional models, the trapped air was less and consequently, the impact pressures greater. In general, when there are mechanisms by which the air may escape, such as a relatively large deadrise on two-dimensional shapes or areas of relatively high curvature on three-dimensional shapes, air entrapment will not be important. For bow flare impact, both of these conditions are met.

The importance of the hydroelastic response of the vessel or experimental model in determining the total impact induced stress has been demonstrated by many researchers. For example, see Belik, et al.[5], Belik and Price[7], Yamamoto, et al.[22], or Toki, et al.[20]. Included in the structural calculations are the external hydrodynamic forces. These hydrodynamic loads may be separated into two separate components: the first due to a rigid body impacting upon the water's surface (an excitation or forcing function), and the second due to the structure's elastic response (a reaction or added mass and damping force). Since the stated purpose of this chapter is to investigate the first kind of force, that associated with rigid body impact, hydroelastic interaction will not be considered except when required to properly interpret experimental results. See, for example, the Appendix of Troesch and Kang [21].

Consider, then, an ideal fluid where a perfectly rigid body passes through the free surface. Additional details of the problem formulation and an alternative solution technique may be found in Troesch and Kang[21]. The free surface is defined by

$$z=\zeta(x,y,t) \tag{1}$$

where (x,y,z) is a right-handed coordinate system with z positive upwards and the origin located at the mean free surface. Newman[16], among others, derived the complete free surface boundary condition, including both kinematic and dynamic considerations, as

$$\frac{\partial^2\phi}{\partial t^2}+g\frac{\partial\phi}{\partial z}+2\nabla\phi\cdot\nabla\frac{\partial\phi}{\partial t}+\frac{1}{2}\nabla\phi\cdot\nabla(\nabla\phi\cdot\nabla\phi)=0 \tag{2}$$

where ϕ is the velocity potential and Eq. (2) must be satisfied on the surface defined by Eq. (1). The governing field equation for potential flow is, of course, the Laplace equation. The body boundary condition, satisfied on the instantaneous body surface, is expressed as

$$\frac{\partial\phi}{\partial n}=\underline{V}\cdot\underline{n} \tag{3}$$

where $\underline{V}$ is the velocity vector of the body and $\underline{n}$ is the outward unit normal. To complete the statement of the above boundary value problem, radiation conditions must be given. Typically these require that the fluid velocity components generated by the body motion approach zero at large distances from the body.

If a velocity potential satisfying the above conditions can be found, then the pressure may be determined from Bernoulli's equation as

$$\frac{p}{\rho}+\frac{\partial\phi}{\partial t}+\frac{1}{2}\nabla\phi\cdot\nabla\phi+gz=\text{const} \tag{4}$$

where g is the gravitational constant. Once the pressure distribution becomes known, it can be integrated and the forces are found in a straight-forward manner.

In this paper, only vertical motion is considered. The velocity vector, $\underline{V}$, used in the body boundary condition is determined from the solution of the equations of motion in the vertical plane shown below:

$$F_z=m\ddot{z}=-\iint p n_z dS \tag{5}$$

The vertical velocity, $\dot{z}(t)$, and displacement, $z(t)$,

are found through the usual integration formulas of

$$\dot{z}(t)=\int_0^t \ddot{z}(t)dt$$
$$z(t)=\int_0^t \dot{z}(t)dt \quad (6)$$

3. Approximate Determination of Impact Forces

A general, three-dimensional solution to the boundary value problem posed in Eqs. (1)~(4) has not yet been found. The complexity of the nonlinear free surface and body boundary conditions requires that simplifying assumptions be made in order to calculate the impact forces. See Greenhow[11] for a detailed review of many of the available methods.

Examination of Eqs. (1)~(4) reveals that both the spatial and temporal variables are possible sources of difficulties. In other words, large changes in time and space are both significant contributors to the physics of impact. Generally, it is possible to catalogue the various existing theories based upon their approximations of the boundary conditions and their assumptions regarding rigid body dynamics. These include, but are not limited to, asymptotic expansions of Eq. (2) with respect to time and space, assumed constant velocity during impact, shallow draft approximations, and assumed two-dimensional behavior. There are extensive literature surveys on the subject elsewhere (i.e. ISSC[27] and ISSC[28]) and they will not be repeated. Rather, a few relevant references will be mentioned here to illustrate the effects of the various assumptions.

The initial efforts to understand impact started with von Karman[26] and was extended by Wagner [24]. Both of these two-dimensional theories used implicit shallow draft approximations and satisfied the equipotential free surface condition of

$$\phi=0 \quad (7)$$

on $z=0$. Wagner[24] derived a "wetting correction" that increased the maximum predicted impact force by a factor of two over von Karman's earlier work. Various extensions to these theories were tried in the following years. Sometimes these extensions were derived in a consistent manner and other times they were not. Armand and Cointe[2] carefully examine the impact forces on a circular cylinder using matched asymptotic expansions. Their results demonstrated that Wagner's wetting correction was indeed valid at the instant of impact, but additional terms were required for later time and larger depths.

With the increase of computational power brought by the introduction of super computers, researchers have attempted to solve the two-dimensional equivalents of Eqs. (1)~(4). The method of choice is based upon the Cauchy integral theorem including the rigid body boundary (Vinje and Brevig [25]) and a mixed Eulerian-Lagrangian description of the free surface (Longuet-Higgins and Cokelet [15]). See, for example, Greenhow and Lin[12], Yim[23], and Greenhow[11]. The differences in the various calculations may be related to the way in which the intersection between the body and free surface is approximated. Reasonable agreement for pressure distributions on small to moderate wedge angles below the mean free surface has been demonstrated. The principal difficulty seems to be in the description of the water jet generated by the impact. Because the method uses complex variables and stream functions, it is difficult to see how this method can be extended to three-dimensions without resorting to some form of strip theory.

If the assumption of constant body velocity is made, then the hydrodynamics of impact may be described by self-similar flows as shown by Shiffman and Spencer[19]. The theory is exact for two-dimensional wedges or three-dimensional axially symmetric cones. Shiffman and Spencer[19] gave an expression for the impact force in terms of the time rate of change of the fluid momentum. To find this momentum, the velocity potential must be integrated over the body boundary and over the exact free surface which generally is not known. Their paper describes a complex iterative procedure by which the solution may be determined and they gave results for a single case—a cone with a 120 degree vertex angle. They concluded that the procedure was too computationally intensive introducing numerical

errors. Consequently, an approximate theory was then suggested which employed elements of Wagner's [24] original work. This approximate theory equated the time rate of change of the fluid momentum to the time derivative of the product of the body velocity and the infinite-fluid added mass. The added mass at any instant was found by increasing the effective draft of the body to account for a wetting correction and then solving the classical infinite fluid boundary value problem. This approach of setting the impact force equal the velocity multiplied by the derivative of the infinite-fluid added mass is fundamentally correct only at the instant of contact when the draft is near zero. However, the method has seen a wide range of applications for deep-draft flare impact loads (Belik, et al. [5] or Yamamoto, et al. [22]).

The reason that it may be a good approximation will be discussed below. The approximate theory of Shiffman and Spencer [19] described above has been extended in curious ways by some researchers. In an effort to get better correlation between theory and experiment, the frequency-dependent added mass has been substituted for the infinite-fluid added mass. See, for example, Beukelman[8]. In that type of impact pressure or impact force calculation, the characteristic frequency is typically based upon the predominant frequency of encounter for the vessel in a seaway. Impact hydrodynamics is clearly a highly nonlinear, transient phenomenon. Under certain circumstances (shallow drafts and small time scales), consistent arguments can be made for the use of the infinite frequency added mass method (Armand and Cointe [2]). However, there is no analytical basis for the use of frequency dependent coefficients which were derived for linear, frequency domain hydrodynamics and that method is not recommended.

The goal of the work presented in this paper is to examine a computationally simple three-dimensional model of bow flare impact. Starting with the free surface condition, Eq. (2), it is assumed that the time duration of impact is much smaller than that normally encountered in normal ship motions. The consequence of this is that time derivatives are relatively large compared to the rest of the terms in Eq. (2). The result is von Karman's [26] free surface condition shown in Eq. (7). The complete body boundary condition of Eq. (3) is retained. Unlike some previous theories that assumed constant velocity during impact, the velocity here is determined from the solution of Eqs. (5) and (6) in incremental time steps. The theoretical model then, has the exact body boundary condition on that part of the body's surface below the mean free surface and the simplified equi-potential free surface condition on $z=0$. This boundary value problem can easily be solved as described by Troesch and Kang [21] or the method outlined in the Appendix A2. A deficiency of the model is its inability to describe any of the hydrodynamic pressure above the mean waterplane, $z=0$. Effects such as spray or jet-like behavior are not present. The extent that this is important in predicting bow flare impact forces will be examined.

In the actual calculations, the boundary value problem described by Eqs. (3) and (7) is solved in a body fixed coordinate system, (x', y', z'). Since Bernoulli's equation is expressed in inertial coordinates, a transformation yields

$$\frac{p(\underline{x}', t)}{\rho} = -\left\{ \frac{\partial \phi(\underline{x}', t)}{\partial t} - \underline{V} \cdot \nabla \phi + \frac{1}{2} \nabla \phi \cdot \nabla \phi + gz \right\} \tag{8}$$

where $p(\underline{x}', t)$ is the pressure in body coordinates and the body velocity vector, $\underline{V}$, has components (U, V, W). The first term of the right-hand side of Eq. (8), $\frac{\partial \phi}{\partial t}$, represents a pressure, that when multiplied by the z-component of the unit normal and integrated over the hull, is equal to the product of the velocity and the time derivative of the added mass. Using this particular term to represent the total impact force, as discussed in the paragraph describing the Shiffman and Spencer [19] method, ignores the convective and quadratic terms of Eq. (8). Troesch and Kang [21] have examined the effect of these two terms for the special cases of a sphere and an axially symmetric body with flare. They found that

the forces associated with these terms are initially small during the first instant of impact. Later, when the total force on the sphere reached its maximum impact value, the two forces became significantly larger, but opposite in sign, thus effectively making only a small net contribution to the impact load. It is not obvious that this type of cancellation is a general characteristic of impact calculations. Consequently, all the terms of Eq. (8) should be used when determining impact pressures.

Another characteristic of state-of-the-art impact theories is the use of two-dimensional calculations coupled with strip theory assumptions to give three-dimensional results. Examples can be found in Ochi and Motter [17] and [18], Yamamoto, et al. [22], Belik and Price [7], Toki, et al. [20], and Bishop, et al. [9]. The usefulness of the slender body or strip theories has long been accepted in normal linear seakeeping analysis. However, the usual seakeeping quantities of interest are global hydrodynamic forces or bending moments and shear forces near the middle of the hull. These forces and moments are typically insensitive to end effects where strip theory approximations are less valid. Bow flare impact and the resulting primary structural loads occur in areas of high longitudinal curvature. The applicability of strip theory in these calculations is questionable. In fact, there is evidence that strip theory in the bow region may overpredict the impact force by a significant amount. Using an example similar to Troesch and Kang's [21] Figure 1, consider the vertical hydrodynamic force acting on a sphere as it passes through a previously undisturbed free surface. To simplify the calculations for this particular example the sphere will be assumed to maintain a constant velocity during impact. The theoretical boundary value problem is represented by Eqs. (3) and (7). The pressure, as given in Eq.(8), is found by both the three-dimensional integral equation method explained in the Appendix A2 or a two-dimensional strip theory. The strip theory just separates the sphere into strips, assumes no interaction between the strips, and for each draft solves a two-dimensional integral equation. The vertical force

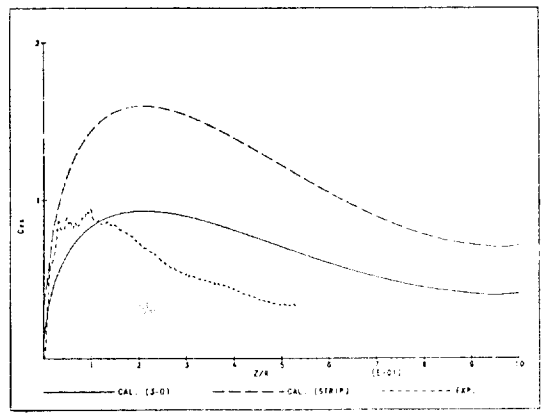

Fig. 1 Experimental and theoretical comparison of the vertical slam coefficient for a sphere. (drop height=61cm (2.0ft))

for both methods was then found by integrating the pressures as shown in Eq. (5). The vertical slam coefficient, C_{vs}, can be defined as

$$C_{vs}=\frac{2m\ddot{z}}{\rho\pi\left(\frac{L}{2}\right)^2 V_0^2} \tag{9}$$

where m is the mass, $\ddot{z}$ is the vertical acceleration, ρ is the water density, L is a representative length, (for the sphere L is the diameter, for the cylindrical body or the flared body it is the overall length). V_0 is the initial vertical impact velocity. Inspection of Eq. (8) shows that all the terms of Bernoulli's equation except for the buoyancy term, gz, may be normalized by the square of the velocity. Consequently, the plots of C_{vs} shown here will become drop height dependent as time and draft increase. Results of the calculations for a drop height of 61cm (2.0ft) along with experimentally measured forces are shown in Fig. 1. The experimental data was taken from Troesch and Kang [21]. Clearly the strip theory approximation is inappropriate for this case. Whether or not this conclusion is also valid for the flared forebody of a ship will be discussed in the next section. There the total vertical impact force, the distribution of the vertical bending moment, and the distribution of the vertical shear force will be computed using two and three-dimensional theories.

4. Presentation of Theoretical and Experimental Results

In order to investigate the validity of the assumptions listed in the previous sections, the hydrodynamic impact forces acting on two different body shapes are examined. The body shapes are shown in Figure 2. One has circular cross sections with a cylindrical parallel midbody. The ends are halves of hemispheres. The other body has a bow flare shape with elliptical water lines. Both shapes have length to beam ratios of 2.0. The cylindrical shape has a beam-to-draft ratio of 2.0 while the flared body has a beam-to-draft ratio of 1.0. Theoretical pressures were calculated by both two-dimensional and three-dimensional boundary integral methods. The three-dimensional method solved the boundary value problem given by Eqs. (3) and (7) and is described in the Appendix A2. The two-dimensional or strip method separated the bodies into vertical segments and applied the two-dimensional equivalents of Eqs. (3) and (7) to the boundaries. Two scale models based upon the lines shown in Figure 2 were built and tested in the Ship Hydrodynamics Laboratory (SHL) at The University of Michigan.

Their principal particulars and the experimental techniques used are listed in the Appendix A1. The vertical impact force as function of time for the cylindrical and flared bodies is shown in Figures 3 and 4 respectively. An approximate drop height of 61cm (2.0 ft) was used. The force has been normalized and is represented by the vertical slam coefficient, C_{vs} of Eq. (9). For both bodies, the overall length is chosen as the characteristic length, L, in C_{vs}. Three different trim angles of 0.0, 5.0, and 10.0 degrees are used. Theoretical calculations based upon the three-dimensional and two-dimensional methods are shown by the solid and short dashed lines respectively. The experimentally measured force is given by the intermediate dashed line. Based upon the information displayed in Figures 3 and 4, the following observations may be made:

(a) The two-dimensional and three-dimensional theoretical curves are surprisingly close when compared to the results for the sphere, a body with a beam to draft ratio of 1.0, shown in Figure 1.

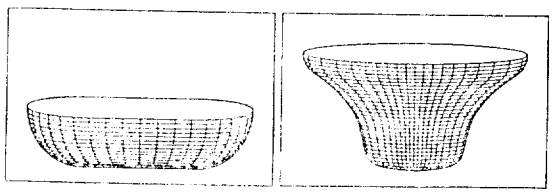

Fig. 2 Panel distribution for the cylindrical and flared bodies

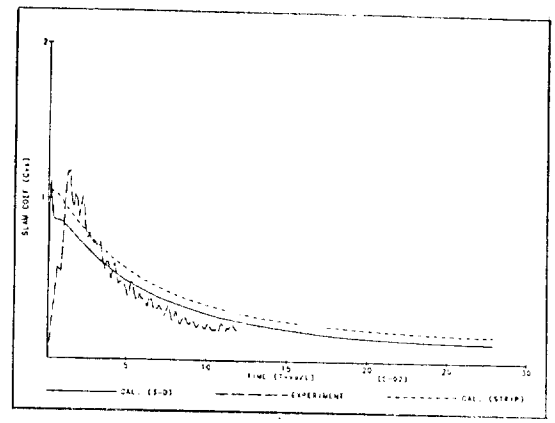

Fig. 3a Experimental and theoretical comparison of the vertical slam coefficient for the cylindrical body (zero degree trim, 61cm (2.0ft) drop height)

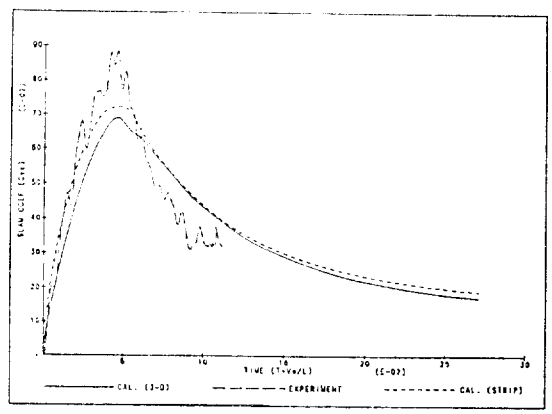

Fig. 3b Experimental and theoretical comparison of the vertical slam coefficient for the cylindrical body (five degree trim, 61cm (2.0ft) drop height)

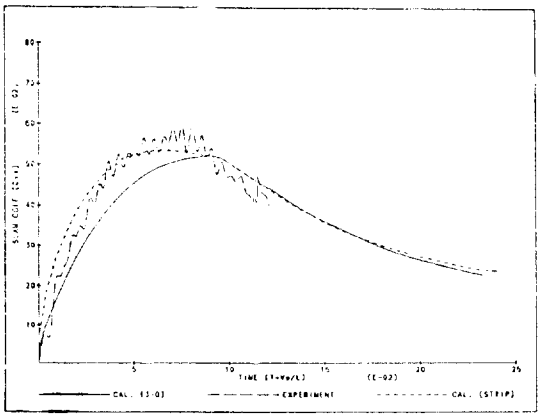

Fig. 3c Experimental and theoretical comparison of the vertical slam coefficient for the cylindrical body (ten degree trim, 61cm (2.0 ft) drop height)

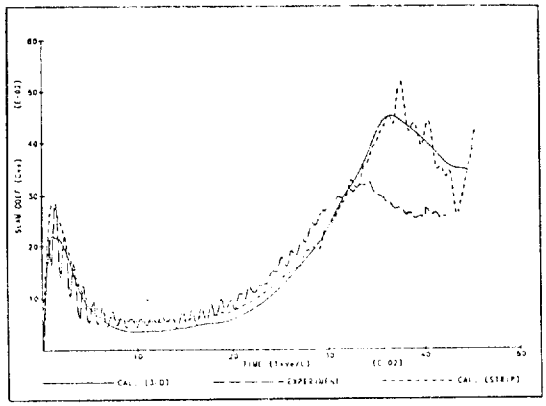

Fig. 4b Experimental and theoretical comparison of the vertical slam coefficient for the flared body (five degree trim, 61cm (2.0 ft) drop height)

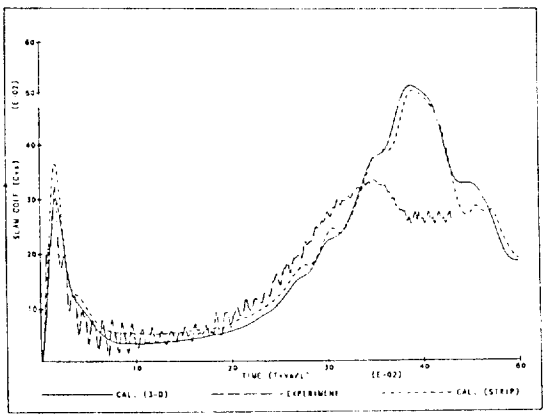

Fig. 4a Experimental and theoretical comparison of the vertical slam coefficient for the flared body (zero degree trim, 61cm (2.0 ft) drop height)

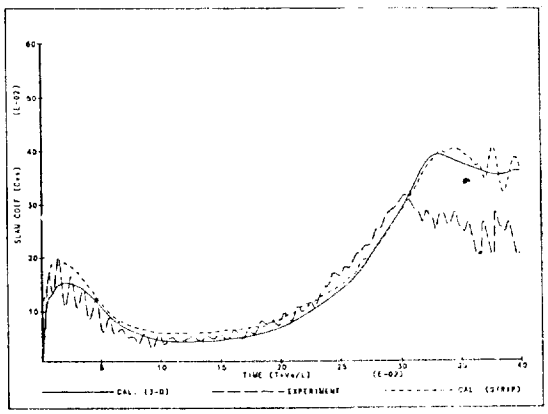

Fig. 4c Experimental and theoretical comparion of the vertical slam coefficient for the flared body (ten degree trim, 61cm (2.0 ft) drop height)

(b) The slam coefficient for the flared body is characterized by two maxima, one occurring during the initial contact between the body and water and the other when the flared sections pass through the surface. The second maximum due to the flare has a value equal to or greater than the first maximum. The results of the strip method in Figs. 4b and 4c show fluctuations after the second maximum. It may be due to numerical instability.

(c) The variation of the trim angle from 0.0 to 10.0 degrees produces a significant decrease in the maximum value of C_{vs} for the cylindrical shape and for the first C_{vs} maximum in the flared body curve. Those C_{vs} values decrease by approximately a factor of two over this range of trim. The decrease due to trim angle change in the second maximum for the flared body is not as large. In fact, the experimental value remains essentially equal for trim angles from 0.0 to 5.0 degrees and then decreases slightly at 10.0 degrees.

(d) The comparison between theory and experiment for the C_{vs} maximum of the cylindrical shape and the first maximum of the flared body is good. However, the second C_{vs} maximum for the flared body was consistently overpredicted, with the largest error occurring at a trim angle of 0.0 degrees and the smallest at 10.0 degrees.

(e) The nondimensional time coordinates for the C_{vs} maxima were underpredicted, predicted correctly, or overpredicted depending upon the body and trim considered.

The experimental results shown in Figures 3 and 4 were representative time histories of a series of impact experiments. The bodies shown in Figure 2 were dropped from three drop heights, 61cm (2.0 ft), 91cm (3.0ft), and 122cm (4.0ft), with three different trim angles, 0.0, 5.0, and 10.0 degrees. Each test condition was conducted at least twice and sometimes as many as five times. The values of the single C_{vs} maximum for the cylindrical shape and the two C_{vs} maxima for the flared body were tabulated and averaged. The slam coefficient maximum for the cylindrical body is due to bottom impact. The two slam coefficient maxima for the flared body are due to bottom impact and flare impact respectively. The averaged C_{vs} values of the maxima for the cylindrical and flared bodies are given in Tables 1 and 2 respectively.

Table 1 Average slam coefficient maxima for the cylindrical body

Drop Height (cm (ft))	Trim Angle (deg)		
	0.0	5.0	10.0
61(2.0)	1.17	0.83	0.55
91(3.0)	1.02	0.85	0.54
122(4.0)	0.90	0.86	0.55

Table 2 Average slam coefficient maxima for the flared body (first maximum/second maximum)

Drop Height (cm (ft))	Trim Angle (deg)		
	0.0	5.0	10.0
61(2.0)	0.30/0.34	0.26/0.34	0.21/0.32
91(3.0)	0.26/0.28	0.24/0.28	0.20/0.26
122(4.0)	0.26/0.26	0.24/0.25	0.21/0.24

Examination of Tables 1 and 2 illustrates some of the uncertainties associated with impact experiments and more generally, with impact hydrodynamics. If the assumptions listed earlier in this paper were valid, such as the assumption that air entrapment was unimportant, then the first maximum of the slam coefficient, C_{vs}, should be invariant with respect to two drop heights. The buoyancy term in Bernoulli's equation, Eq. (8), is effectively zero and the remaining dynamic terms can be normalized by the

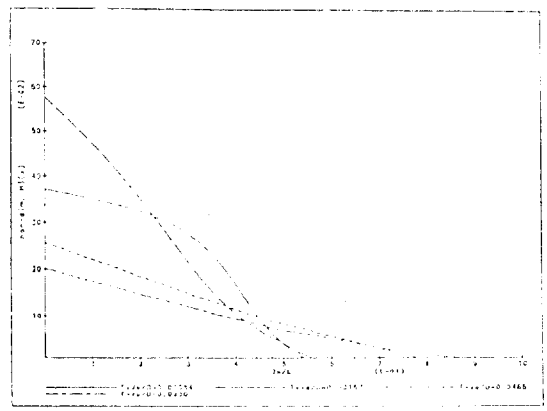

Fig. 5a Theoretical hydrodynamic shear distribution at various nondimensional times for the cylindrical body (Zero degree trim)

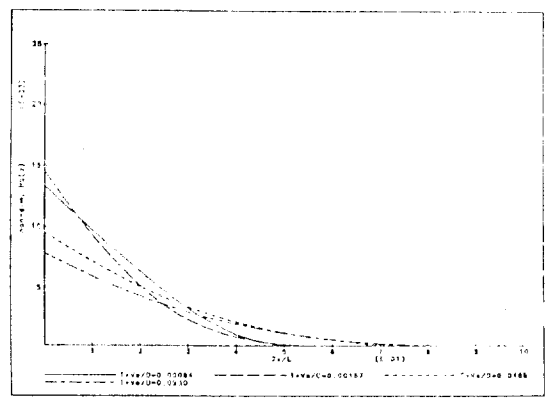

Fig. 5b Theoretical hydrodynamic bending moment distribution at various nondimensional times for the cylindrical body (Zero degree trim)

velocity squared. Tables 1 and 2 show that this is only true when the trim angle is not zero. For trim angles of 5.0 and 10.0 degrees, the slam coefficients are effectively independent of drop height which is proportional to the initial velocity squared. For a trim angle of 0.0 degrees, the slam coefficient decreases as the drop height or velocity increases. Chuang and Milne [10] suggest that this may be a characteristic of air entrapment. Clearly small changes in body geometry or entry angle can have a large effect upon the amount of air that is pushed aside and upon the subsequent impact load.

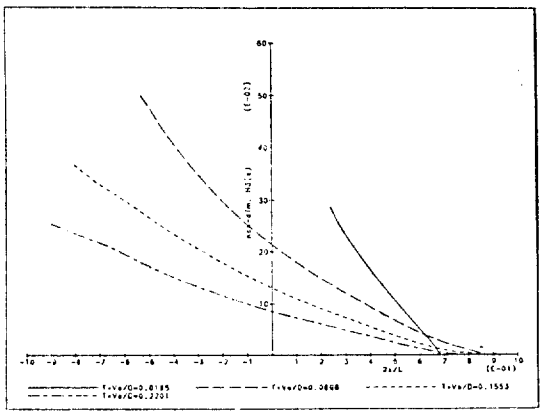

Fig. 6a Theoretical hydrodynamic shear distribution at various nondimensional times for the cylindrical body (ten degree trim)

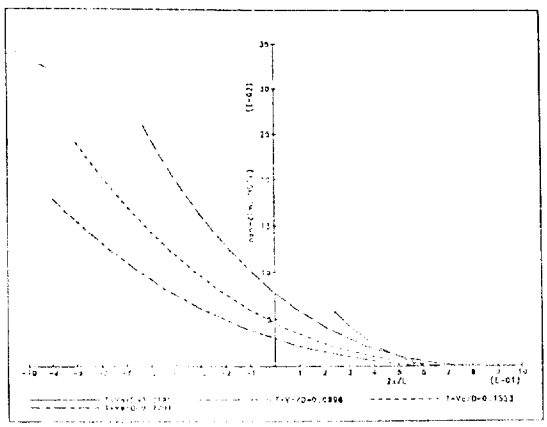

Fig. 6b Theoretical hydrodynamic bending moment distribution at various nondimensional times for the cylindrical body (ten degree trim)

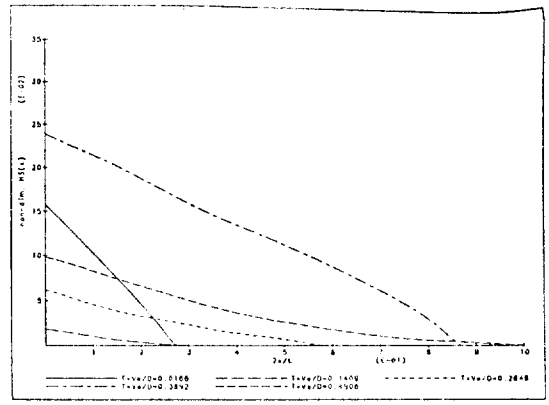

Fig. 7a Theoretical hydrodynamic shear distribution at various nondimensional times for the flared body (zero degree trim)

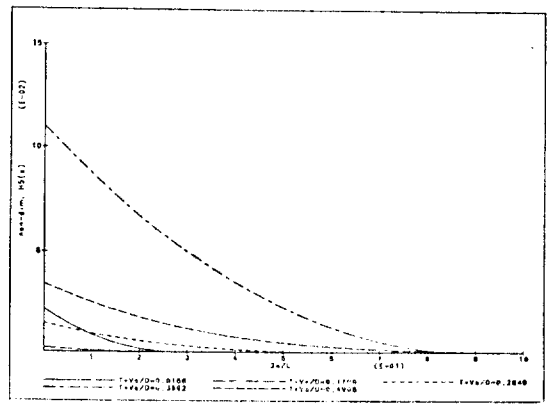

Fig. 7b Theoretical hydrodynamic bending moment distribution at various nondimensional times for the flared body (zero degree trim)

Given the mass distribution of the body and the pressure distribution as shown in Eq. (8), the vertical shear, $V_3(x)$, and vertical bending moment, $M_5(x)$, can be determined by the following:

$$V_3(x)=I_3(x)-H_3(x)$$
$$M_5(x)=I_5(x)-H_5(x)$$
$$I_3(x)=\int_x^{L/2} m(x')a(x')dx'$$
$$H_3(x)=\int_x^{L/2}\int_{C(x')} pn_3 dS$$
$$I_5(x)=-\int_x^{L/2}(x'-x)m(x')a(x')dx'$$
$$H_5(x)=\int_x^{L/2}\int_{C(x')} pn_3(x'-x)dS \qquad (10)$$

where $I_3(x)$ and $I_5(x)$ are the inertial force and moment respectively, $H_3(x)$ and $H_5(x)$ are the hydrodynamic force and moment respectively, $m(x')$ is sectional mass distribution, $C(x')$ is the hull section contour at station x', and $a(x')$ is the local section acceleration at station x'. Since the inertial loads are functions of the mass distribution and independent of the hydrodynamics, they will not be included in the calculations shown here.

The hydrodynamic shear, $H_3(x)$, and moment, $H_5(x)$, are shown in Fig. 5 through 11. The hydrodynamic shear and moment are not zero at the ends. They have been normalized by $1/2\rho\pi(L/2)^2 V_0^2$ and $1/2\rho\pi(L/2)^3 V_0^2$ respectively. In Fig. 5 through 8, the shear and bending moment for the two bodies at selected values of the nondimensional time variable, $T^* V_0/D$ are shown. The trim angles in Fig. 5 and 7 are 0.0 degrees and in Fig. 6 and 8, 10.0 degrees. Due to the symmetry of the forces for impact at zero trim, the shear and moment are only shown for values of x from zero to $L/2$ in Fig. 5 or 7.

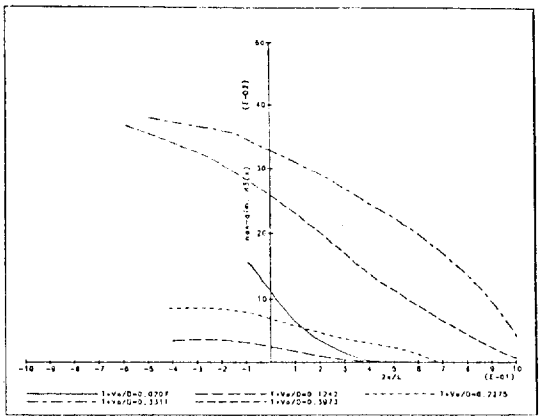

Fig. 8a Theoretical hydrodynamic shear distribution at various nondimensional times for the flared body (ten degree trim)

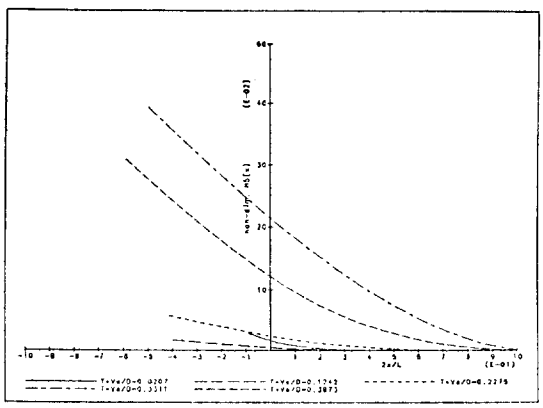

Fig. 8b Theoretical hydrodynamic bending moment distribution at various nondimensional times for the flared body (ten degree trim)

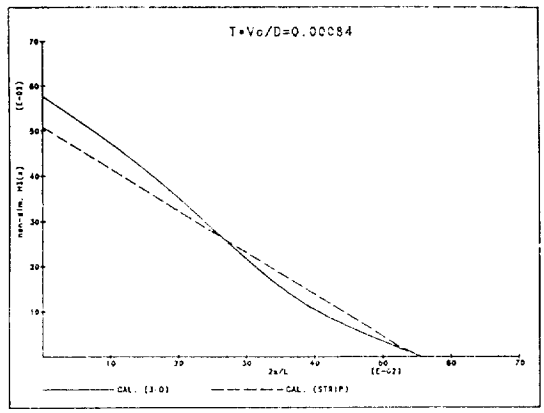

Fig. 9a Comparison between 3-D and strip theory calculations of the hydrodynamic shear distribution for the cylindrical body taken at time of maximum impact force (0 trim)

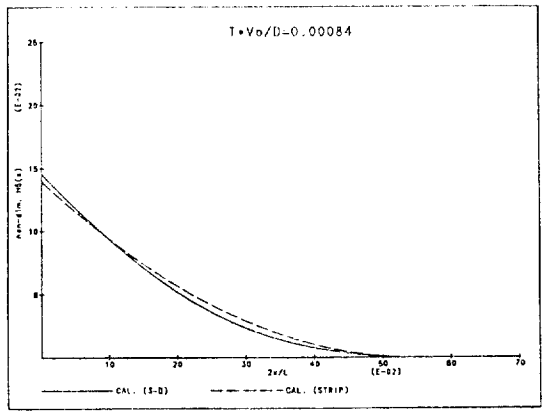

Fig. 9b Comparison between 3-D and strip theory calculations of the hydrodynamic bending moment distribution for the cylindribal body taken at time of maximum impact force (0 trim)

The different figures show that the time of overall maximum impact does not necessarily correspond to the time of maximum shear or bending moment. For a given initial approach velocity, the time of maximum hydrodynamic shear or moment, depends upon the geometry of the body, the trim angle, and the station at which the force or moment is desired. As an example, consider the shear and bending moment at an x coordinate of $2x/L=0.0$ for the flared body. This is analogous to the shear and moment acting in a vessel with large flare at

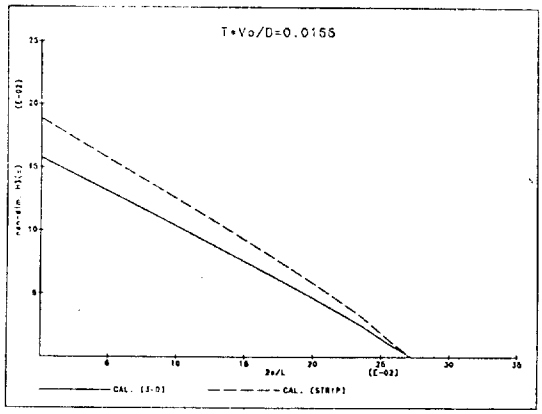

Fig. 10a Comparison between 3-D and strip theory calculations of the hydrodynamic shear distribution for the flared body taken at time of first maximum impact force (0 trim)

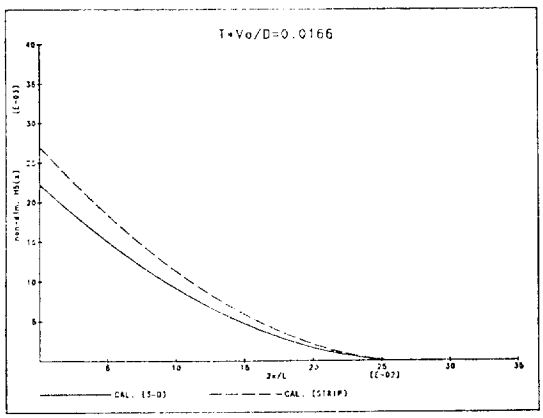

Fig. 10b Comparison between 3-D and strip theory calculations of the hydrodynamic bending moment distribution for the flared body taken at time of first maximum impact force (0 trim)

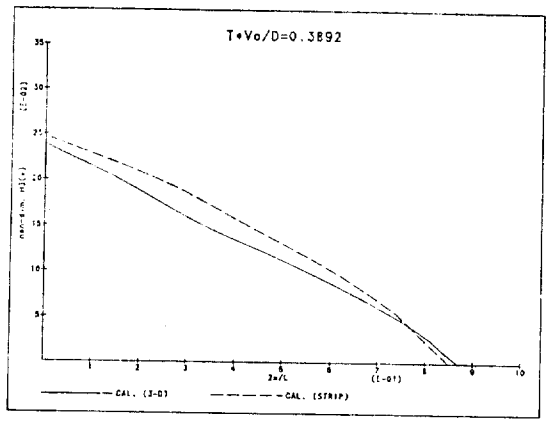

Fig. 11a Comparison between 3-D and strip theory calculations of the hydrodynamic shear distribution for the flared body taken at time of second maximum impact force (0 trim)

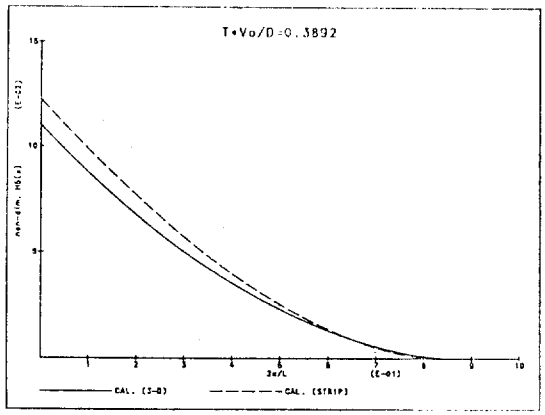

Fig. 11b Comparison between 3-D and strip theory calculations of the hydrodynamic bending moment distribution for the flared body taken at time of second maximum impact force (0 trim)

a distance less than one beam aft of the forward perpendicular. Generally, the impact loads corresponding to the first maximum of the slam coefficient curve will produce higher local pressures than the second maximum. This follows since the magnitude of the first C_{vs} maximum is of the same order as the second C_{vs} maximum but is acting over a smaller area. The trend in the bending moments resulting from those maxima, however, is in the opposite direction. When the trim angle is zero, the moment

associated with the second maximum is approximately five times as large as that associated with the first maximum. When the trim angle is ten degrees, the ratio of these in moments becomes approximately ten to one. This implies that there two different hydrodynamic impact loading conditions for forebody structural analysis-one for the design of the shell plating to withstand local impact pressures and one for the design of the hull girder to withstand global impact loads. Both should be investigated in order to insure an adequate ship design.

Comparisons between the two-dimensional strip calculations and the three-dimensional calculations are shown in Figs. 9, 10, and 11. The nondimensional times were selected to correspond to the maxima in the slam coefficient curves. The cylindrical body results are shown in Fig. 9 while flared body results are shown in Fig. 10 and 11. As in the slam coefficient figures, Fig. 3 and 4, the strip theory values are greater than the three-dimensional ones, but not nearly as much as might have been expected based upon the curves shown in Fig. 1.

5. Summary and Conclusions

Hydrodynamic loads due to flare impact have been examined. A simplified theory using the equipotential free surface boundary condition of von Karman[26] has been presented. Based upon the results of the analysis presented here, the following conclusions may be drawn:

(a) The approximate added mass method of Wagner[24] and Shiffman and Spencer[19] are strictly valid only for bottom slamming. For bow flare or hydrodynamic loads on non-zero draft sections, the analysis should include the complete form of Bernoulli's equation.

(b) The exact body boundary condition plus von Karman's[26] equipotential free surface condition give adequate engineering predictions for three-dimensional bottom impact loads, but overpredict the impact load due to flare. The overprediction was greatest for the zero trim condition and decreased as the trim angle increased. This overprediction is principally a result of using the simplified free surface boundary condition which neglects the jet-like behavior of the water.

(c) Computations based upon strip theory compare closely with those from the equivalent three-dimensional theory when the beam to draft ratio equals or exceeds 2.0. The same conclusion applies to the vertical bending moment and shear in the bow region. This can provide a significant savings in impact calculations since strip theories are easier to implement than three-dimensional formulas.

(d) The impact load, shear, or bending moment due to bow flare can equal or exceed that due to bottom slamming. While bottom slamming may result in higher local pressures, relatively lower flare impact pressures, spread over a larger surface, can produce larger loads and moments.

(e) A slight change in the relative angle between the hull surface and water can significantly change the impact force. The maximum theoretical force occurs at zero relative trim angle and decreases as the angle increases. This trend is supported by experimental data, though air entrapment seems to be a significant factor for impact at near zero angles.

Acknowledgments

This work was primarily supported by the Maritime Administration University Research Program, contract DTMA91-86-C-60120, and The University of Michigan Rackham Pre-doctoral Fellowship. Acknowledgement is also given to the David Taylor Research Center, Bethesda, Maryland, U.S.A. and Korea Research Institute of Ships and Ocean Engineering (KRISO).

References

[1] Abramowitz, M. & Stegun, I.A., Handbook of Mathematical Functions, Government Printing Office, Washington, 1964.

[2] Armand, J.L., and Cointe, R., "Hydrodynamic Impact Analysis of a Circular Cylinder", *Proceedings, 5th OMAE Symp.*, Tokyo, 1986.

[3] Barsky, B.A., "End Conditions and Boundary Conditions for Uniform B-Spline Curve and Surface Representations", Computers in Industry 3, pp. 17-29, 1982.

[4] Barsky, B.A. & Greenberg, D.P., "Determining a Set of B-Spline Control Vertices to Generate an Interpolating Surface", Computer Graphics and Image Process 14, pp. 203-226, 1980.

[5] Belik, O., Bishop, R.E.D. and Price, W.G., "On the Slamming Response of the Ships to Regular Head Waves", *Trans. RINA.*, 122, 1980.

[6] Belik, O., Bishop, R.E.D. and Price, W.G., "A Simulation of Ship Responses Due to Slamming in Irregular Head Seas", *Trans. RINA*, 125, 1983.

[7] Belik, O., and Price, W.G., "Comparison of Slamming Theories in the Time Simulation of Ship Responses in Irregular Waves", Int. Shipb. Prog., 29, 1982.

[8] Beukelman, W., "Bottom Impact Pressures Due to Forced Oscillation", Int. Shipb. Progr., 27, 1980.

[9] Bishop, R.E.D., Clarke, J.D., and Price, W.G., "Comparison of Full Scale and Predicted Responses of Two Frigates in a Severe Weather Trail", *Trans. RINA*, 126, 1984.

[10] Chuang, S.-L., and Milne, D., "Drop Tests to Investigate the Three-Dimensional Effects of Slamming", NSRDC Report 3543, 1971.

[11] Greenhow, M., "Wedge Entry Into Initially Calm Water", Applied Ocean Res., Vol. 9, No. 4, 1987.

[12] Greenhow, M. and Lin, W.-M., "Numerical Simulation of Nonlinear Free Surface Flows Generated by Wedge Entry and Wavemaker Motions", *Proc. 4th Int. Conf. Num. Ship H-dro.*, Washington D.C., 1985.

[13] Kaplan, W., Advanced Mathematics for Engineers, Addison-Wesley Publishing Co., 1981.

[14] Lin, W.-M., "Nonlinear motion of the free surface near a moving body," Ph.D. Thesis, M.I.T., Dept. of Ocean Engineering, Cambridge, MA, 1984.

[15] Longuet-Higgins, M.S., and Cokelet, E.D., "The Deformation of Steep Surface Waves on Water. I. A Numerical Method of Computation", Proc. Roy. Soc. Lon., 350, 1, 1976.

[16] Newman, J.N., Marine Hydrodynamics, MIT press, Cambridge, MA, 1977.

[17] Ochi, M.K. and Motter, L.E., "Prediction of Extreme Values of Impact Pressure Associated with Ship Slamming", *Jour. of Ship Res.*, Vol. 13, No. 2, 1969.

[18] Ochi, M.K. and Motter, L.E., "Prediction of Slamming Characteristics and Hull Responses for Ship Design", *SNAME Trans.*, pp. 144-176, 1973.

[19] Shiffman, M. and Spencer, D.C., "The Forces of Impact on a Cone Striking a Wtaer Surface", *Comm. Pure Appl. Math.*, Vol. 4, pp. 379-417, 1951.

[20] Toki, N., Hatakenaka, K., Takahashi, T. and Fujii, H., "Experimental and Theoretical Approach to the Estimation of Non-Linear Vertical Wave Loads", Autumn Meeting, *Jour. Soc. Naval Arch. Japan*, 1983.

[21] Troesch, A.W., and Kang, C.-G., "Hydrodynamic Impact Loads on Three-Dimensional Bodies", *16th Symp. on Naval Hydro.*, Berkeley, 1986.

[22] Yamamoto, Y., Ohtsubo, H., Takeda, Y., Fukasawa, T., "Structural Failure of a Small Cargo Vessel Among Rough Seas", Extreme Loads Response Symposium, SSC and SNAME, Arlington, VA, 1981.

[23] Yim, B., "Numerical Solution for Two-Dimensional Wedge Slamming With a Nonlinear Free Surface Condition", *Proc. 4th Int. Conf. Num. Ship Hydro.*, Washington D. C, 1985.

[24] Wagner, H., "Landing of Seaplanes", NACA TN 622, 1931.

[25] Vinje, T. and Brevig, P., "Nonlinear Two-dimensional Ship Motions", *Proc. 3rd Int. Conf. Num. Ship Hydro.*, Paris, 1980.

[26] von Karman, T., "The Impact on Seaplane Floats During Landing", NACATN 321, 1929.

[27] 8th International Ship Structures Congress., Report of Committee II. 3: "Transient Dynamic

Loadings and Response", Gdansk, 1982.
[28] 9th International Ship Structures Congress., Report of Committee II.3: "Transient Dynamic Loadings and Response", Genova", Genova, 1985.

Appendix A1 Impact Experiments

Impact experiments were conducted in the Ship Hydrodynamics Laboratory located at The University of Michigan, Ann Arbor, Michigan. Two models were dropped from various heights. The model geometries are shown in Figure 2 and the model particulars are shown below in Table 3. The models were dropped from three drop heights, 61cm (2.0ft), 91cm (3.0ft) and 122cm (4.0ft), with three different trim angles, 0.0, 5.0, and 10.0 degrees.

The vertical acceleration was measured with a PCB Piezotronics Inc. Piezoelectric accelerometer, model no. 302A02. This accelerometer has a natural frequency greater than 35KHz and was attached to a steel plate installed into the base of the models. The models were constructed of solid sugar pine in order to make them as stiff as possible. The total system had many natural frequencies reflecting the elastic nature of the composite wood and steel construction. Spectral analysis revealed that the first natural frequency was in the range of 400 to 450Hz with subsequent ones starting at approximately 1000 Hz. The accelerometer signals were digitized at a sampling rate of 21 KHz and numerically filtered with a cutoff frequency of 800 Hz. The filtered result was then analyzed using the single degree-of-freedom technique described in the Appendix of Troesch and Kang [21]. The maximum impact accelerations, which are directly proportional to the maximum impact forces, were then read from the resulting time histories.

Table 3 Experimental model particulars

	Cylindrical Body	Flared Body
Length	76.2cm (2.5ft)	76.2cm (2.5ft)
Beam	38.1cm (1.25ft)	38.1cm (1.25ft)
Draft	19.1cm (0.625ft)	38.1cm (1.25ft)
Weight	350.1N (78.70lbs)	356.7N (80.20lbs)

Appendix A2 Theoretical and Computational Datail

Consider a body with bounding surfaces and outward unit normal $\underline{n}$. The fluid domain is R. The bounding surfaces on the free surface, body, and at infinity are given as S_f, S_b, and S_∞. The Governing equations for the velocity potential, $\phi(\underline{x})$, and a Green function $G(\underline{x}, \underline{y})$, are

$$\nabla^2\phi(\underline{x})=0$$
$$\nabla^2 G(\underline{x}, \underline{y})=-\delta(\underline{x}-\underline{y}) \tag{11}$$

where $\underline{x}$ is the vector to the field point, $\underline{y}$ is the vector to the source point, and $\delta(\underline{x}-\underline{y})$ is the Dirac delta function. Through the application of Green's second identity in R the potential is given as

$$\alpha(\underline{x}, t)\phi(\underline{x}, t)=\iint_{S_b+S_f+S_\infty}\left\{\frac{\partial\phi}{\partial n}-\phi\frac{\partial}{\partial n}\right\}GdS \tag{12}$$

where α is an included angle. For the pressure release problem, the appropriate Green function is

$$G(\underline{x}, \underline{y})=\frac{1}{|\underline{x}-\underline{y}|}-\frac{1}{|\underline{x}-\underline{y}'|} \tag{13}$$

where $\underline{y}'$ is an image of $\underline{y}$ about $z=0$. Since both $G(\underline{x}, \underline{y})$ and $\phi(\underline{x})$ are zero on S_f and both go to zero at a sufficient rate far from the body, the integrals on S_f and S_∞ contribute nothing in Eq. (12).

The body surface is discretized into the small surface elements ΔS_{ij} (see, for example, Fig. 2) using a bilinear cubic B-spline algorithm (Barsky & Greenberg [4] and Barsky [3]). The surfaces ΔS_{ij} can be represented by the parameters, u and v. Thus

$$x=f(u, v),\ y=g(u, v),\ z=h(u, v) \text{ for } 0\leq u\leq 1 \text{ and } 0\leq v\leq 1.$$

This allows the curved panels. The boundary values of ϕ and $\frac{\partial\phi}{\partial n}$ are assumed to be bilinear on the subdivided surface ΔS_{ij} as shown below.

$$\phi=a_0+a_1u+a_2v+a_3uv \text{ and}$$
$$\frac{\partial\phi}{\partial n}=b_0+b_1u+b_2v+b_3uv$$
$$\text{for } 0\leq u\leq 1 \text{ and } 0\leq v\leq 1 \tag{14}$$

The surface integral of Eq. (12) is evaluated by using 4-point Gaussian quadrature for the adjacent elements to the point at which the boundary conditions are applied, or by using 2-point Gaussian quadrature for the rest of the segments. The weighting factors and abscissas for Gaussian quadratures are given in Abramowitz & Stegun [1]. The surface integration and the calculation of the normal vector on the surface are described in Appendix A3. So, the simultaneous equations for ϕ_{ij} can be obtained from Eq. (12).

If the body motion is given, pressures, forces, and moments on a body can be calculated without using of a complex numerical integration scheme like Runge-Kutta. In addition, if the body motion is purely translational, the dipole distribution method described by Troesch and Kang[21] can be used rather than relatively complicated direct method of Eq. (12). But when the body motion is unknown and may include rotational motion, a complex numerical integration scheme is required. In this paper the fourth order Runge-Kutta scheme is employed for time integration. From fundamental rigid body dynamics we have the following relations:

$$\frac{\delta \underline{n}}{dt}=\underline{\omega}\times\underline{n} \tag{15}$$

$$\frac{\delta(\underline{n}\phi)}{dt}=\phi\frac{\delta \underline{n}}{dt}+\underline{n}\frac{\delta\phi}{dt} \tag{16}$$

where $\frac{\delta}{dt}$ represents the time derivatives in the non-inertial body coordinate system and $\underline{\omega}$ is an angular velocity vector. In order to calculate the pressure on the body, the time derivative of the potentials required as shown in Eq.(8). Since ϕ for $t\leq t_n$ is known, only a backward difference formula can be used to get $\frac{\delta\phi}{dt}$ at $t=t_n$. But this explicit time stepping formula may experience stability difficulties. As an alternative consider the following form of Eq. (9).

$$\begin{aligned}\underline{F}&=m\dot{\underline{V}}\\&=\iint_S p\underline{n}dS-mg\underline{k}\\&=-\iint_S \underline{n}\left(\frac{\delta\phi}{dt}-\underline{V}\cdot\nabla\phi+\frac{1}{2}\nabla\phi\cdot\nabla\phi+gz\right)dS\\&\quad -mg\underline{k}\end{aligned} \tag{17}$$

In the above equation the fluid velocity can be calculated numerically by using the potential on the body surface. The fluid velocity near $z=0$ was approximated as the fluid velocity at 10% girth length from $z=0$ because the fluid velocity near $z=0$ is singular unless the intersection angle is 90 degrees. Substituting Eq.(15) and (16) into Eq. (17) yields the following equation.

$$\begin{aligned}m\dot{\underline{V}}=&-\rho\frac{\partial}{\partial t}\iint_S \underline{n}\phi dS-mg\underline{k}\\&-\rho\iint_S\left[-\phi\underline{\omega}\times\underline{n}-\underline{n}\underline{V}\cdot\nabla\phi\right.\\&\left.+\frac{1}{2}\nabla\phi\cdot\nabla\phi\underline{n}+gz\underline{n}\right]dS\end{aligned} \tag{18}$$

Define

$$\underline{p}_1\equiv m\underline{V}+\rho\iint_S \underline{n}\phi dS+mg(t-t_0)\underline{k} \tag{19}$$

It follows

$$\dot{\underline{p}}_1=-\rho\iint_S\left[-\phi\underline{\omega}\times\underline{n}-\underline{n}\underline{V}\cdot\nabla\phi+\frac{1}{2}\nabla\phi\cdot\nabla\phi\underline{n}+gz\underline{n}\right]dS \tag{20}$$

with an initial condition

$$\underline{p}_1(0)=m\underline{V}(0)+\rho\iint_{S(0)}\underline{n}\phi dS+mgt_0\underline{k} \tag{21}$$

Similarly for the angular motion,

$$\underline{H}_1\equiv\underline{H}+\rho\iint_S \underline{r}\times\underline{n}\phi dS \tag{22}$$

$$\begin{aligned}\dot{\underline{H}}_1=&-\rho\iint_S\left[-\phi(\underline{r}\times\underline{n})\times\underline{\omega}+(\underline{r}\times\underline{n})\right.\\&\left.\left(-\underline{V}\cdot\nabla\phi+\frac{1}{2}\nabla\phi\cdot\nabla\phi+gz\right)\right]dS\end{aligned} \tag{23}$$

with an initial condition

$$\underline{H}_1(0)=\underline{H}(0)+\rho\iint_{S(0)}\underline{r}\times\underline{n}\phi dS \tag{24}$$

where $\underline{H}$ is the angular momentum of a rigid body.

After $\underline{p}_1$ and $\underline{H}_1$ are obtained by applying the fourth order Runge-Kutta scheme, $\underline{V}$ and $\underline{\omega}$ can be calculated from eq.(19) and eq.(22). The advantage of this technique does not require the explicit time derivative of the potential. Note the first term of Eq. (18) is the time derivative of the classical added mass frequently used in impact calculation and the added mass multiplied by acceleration. The method represented by Eq. (18) and Eqs. (19) and (20) were both used calculating the results shown in this paper.

A simple method can be introduced by using Eq. (18) if the body motion is given and is translational in z-direction. First, the added mass and each inte-

gral in Eq. (18) may be calculated and stored for small changes in the body geometry. Second, take the derivative of the added mass in z-direction and get a term of the first integral in Eq. (18). Third, all of the hydrodynamic terms can be normalized by U^2L^2. The body motion can be simulated by using the interpolation of the obtained hydrodynamic and hydrostatic terms. The potentials at the three time steps are needed to get the time derivative of the potential in Eq. (17) by using the central difference scheme. The boundary value problems at the three time time steps are solved by using the results of the simulation. Finally, the shear force and bending moment at the given time can be obtained by integrating the pressures calculated from the solutions of the boundary value problem.

Appendix A3 Calculation of the Surface Integral and the Normal Vector

The surface integral can be calculated as follows (Kaplan, 1981):

$$\iint_S H(x,y,z)\ d\sigma=\iint_{S_{uv}} H[f(u,v),\ g(u,v),\ h(u,v)]\ \sqrt{EG-F^2}\,dudv \tag{25}$$

where

$$x=f(u,v),\quad y=g(u,v),\quad z=h(u,v)$$

$$\underline{P}_1=x_u\underline{i}+y_u\underline{j}+z_u\underline{k}$$

$$\underline{P}_2=x_v\underline{i}+y_v\underline{j}+z_v\underline{k}$$

$$E=|\underline{P}_1|^2=\left(\frac{\partial x}{\partial u}\right)^2+\left(\frac{\partial y}{\partial u}\right)^2+\left(\frac{\partial z}{\partial u}\right)^2$$

$$F=\underline{P}_1\cdot\underline{P}_2=\frac{\partial x}{\partial u}\frac{\partial x}{\partial v}+\frac{\partial y}{\partial u}\frac{\partial y}{\partial v}+\frac{\partial z}{\partial u}\frac{\partial z}{\partial v}$$

$$G=|\underline{P}_2|^2=\left(\frac{\partial x}{\partial v}\right)^2+\left(\frac{\partial y}{\partial v}\right)^2+\left(\frac{\partial z}{\partial v}\right)^2$$

The normal vector on the surface S is calculated by using the following formula.

$$\underline{n}=\frac{\underline{P}_1\times\underline{P}_2}{|\underline{P}_1\times\underline{P}_2|} \tag{26}$$